Evaluation Method for Fieldlike-Torque Efficiency by Modulation of the Resonance Field

Changsoo Kim, Dongseuk Kim, Byong Sun Chun, Kyoung-Woong Moon, and Chanyong Hwang*
Spin Convergence Research Team, Korea Research Institute of Standards and Science, Daejeon 34113, Republic of Korea

(Received 20 November 2017; revised manuscript received 1 March 2018; published 24 May 2018)

The spin Hall effect has attracted a lot of interest in spintronics because it offers the possibility of a faster switching route with an electric current than with a spin-transfer-torque device. Recently, fieldlike spin-orbit torque has been shown to play an important role in the magnetization switching mechanism. However, there is no simple method for observing the fieldlike spin-orbit torque efficiency. We suggest a method for measuring fieldlike spin-orbit torque using a linear change in the resonance field in spectra of direct-current (dc)-tuned spin-torque ferromagnetic resonance. The fieldlike spin-orbit torque efficiency can be obtained in both a macrospin simulation and in experiments by simply subtracting the Oersted field from the shifted amount of resonance field. This method analyzes the effect of fieldlike torque using dc in a normal metal; therefore, only the dc resistivity and the dimensions of each layer are considered in estimating the fieldlike spin-torque efficiency. The evaluation of fieldlike-torque efficiency of a newly emerging material by modulation of the resonance field provides a shortcut in the development of an alternative magnetization switching device.

DOI: 10.1103/PhysRevApplied.9.054035

I. INTRODUCTION

Ferromagnetic resonance (FMR) is a phenomenon in which the precession amplitude of magnetization reaches a maximum when the frequency of an applied microwave (MW) magnetic field generating a driving torque in the magnetization meets with the precession frequency of a ferromagnet's (FM's) magnetization in an external magnetic field. When resonance occurs, there is a phase difference of $\pi/2$ between the driving torque and the magnetization in the resonance magnetic field (or MW resonance frequency). Normally, a physical system is analyzed through the resonance field (or the MW resonance frequency) and the absorption linewidth in a FMR spectrum.

Among several FMR techniques, the spin-torque FMR (ST FMR) has been developed to investigate spin-transfer torque in a magnetic tunnel junction [1–4]. Recently, the ST-FMR technique has been widely used in spin-orbit torque (SOT) research to measure torques in a FM/normal metal (NM) bilayer structure [5,6]. Within a NM that shows a large spin-orbit coupling, there is a spin-current flow perpendicular to the direction of the electrical current, which results in the transfer of fieldlike SOT (FLT) and dampinglike SOT (DLT) to magnetization [7–12]. In ST FMR, a MW current applied to a NM layer generates an Oersted torque as well as SOT. When these torques oscillating with an applied MW frequency resonate the precession motion of the magnetization under a magnetic field, the amplitude of the precession motion of the magnetization reaches a maximum. The oscillating amplitude of resistance induced by the anisotropic magnetoresistance and the spin Hall magnetoresistance also increases and is mixed with the MW current simultaneously; therefore, the ST-FMR spectrum affected by SOT can be measured in a direct-current (dc) voltage [3].

As the line shape in the ST-FMR spectrum includes information about SOT, various methods have been suggested for SOT analysis: e.g., using the intensities of symmetric and antisymmetric Lorentzian curves, a non-FLT model [5], FM layers of varying thickness [12], and experimentally estimated MW current [13,14]. The amplitude of the MW current has to be considered in line-shape analysis. In the model without FLT, DLT efficiency (DLTE; ξ_{DL}) can be estimated from dividing the DLT by the Oersted torque instead of obtaining the value of the MW current. Of course, the line-shape analysis fails if there is FLT parallel to the Oersted torque. In a FM/NM bilayer system with SOT, the changing thickness of the FM layer means a change of the ratio between the Oersted torque and the SOT. Though FLT efficiency (FLTE; ξ_{FL}) and DLTE can be estimated from various thicknesses of the FM layer, this method assumes that all devices have the same physical properties. With MW current estimated from a complex microwave model of a ST-FMR device, verifying the MW model would be a problem. Moreover, induced voltage from the inverse spin Hall effect can alter the signal of ST FMR because the line-shape methods analyze the signal intensities of two Lorentzians [15,16].

*cyhwang@kriss.re.kr

Here, we consider the effect of FLT in a dc-tuned ST FMR to investigate the SOT of a FM/NM bilayer structure in a simulation and in experiments. We obtain FLTE by analyzing the modulation of the resonance field (MOR) in the spectra of ST FMR. After a thermal effect of a direct current is removed from shift of resonance field, the effective field of a FLT by a dc is estimated by subtracting the Oersted field from the shift in the resonance field. Also, we study the precession phase of magnetization, which is determined by the oscillating FLT, DLT, and Oersted torque in a resonance magnetic field of various FM thicknesses. Moreover, we compare two values of FLTE which are estimated from different schemes. The aim of this article is the introduction of an evaluation method of FLTE. Thus, we do not discuss the spin-diffusion length or the bulk spin Hall angle of tungsten.

II. RESULTS AND DISCUSSION

In the ST-FMR experiment depicted in Fig. 1(a), the Oersted torque, DLT, and FLT generated from Ampere's law, and the spin Hall effect (SHE) by the MW current, lead to the FMR in the magnetic layer [Fig. 1(b)]. If we apply a dc, these three torques are also generated by a dc. Among them, DLT enhances damping or antidamping depending on the transferred spin direction during the resonance, which results in changes in the absorption linewidth [17]. The effective fields of the FLT and the Oersted field are perpendicular to the dc and are aligned in the plane of the thin film. Thus, the total static field ($\boldsymbol{H}_{\text{tot static}}$) applied to the magnetization can be expressed as

$$\boldsymbol{H}_{\text{tot static}} = \boldsymbol{H}_{\text{ext}} + \boldsymbol{H}_{\text{Oe,dc}} + \boldsymbol{H}_{\text{FLT,dc}}, \tag{1}$$

where $\boldsymbol{H}_{\text{ext}}$, $\boldsymbol{H}_{\text{Oe,dc}}$, and $\boldsymbol{H}_{\text{FLT,dc}}$ are the external magnetic field, the Oersted field, and the effective field of FLT by the dc in the NM [Fig. 1(c)]. Thus, in the dc-tuned ST FMR, the shifted resonance field $[\Delta H_R(I) = H_R(I) - H_R(I=0)]$ is the amount of vector projection of the effective field of the FLT and the Oersted field on the external magnetic field (>10 mT) because two fields by a dc (approximately 10 mA) are below 1 mT in a normal ST-FMR device (about 20-μm wide and approximately 5 nm thick), where $H_R(I)$ is the resonance field at the dc (I) applied to the device. Thus, Eq. (1) can be expressed as

$$\Delta H_R = -(\Delta H_{\text{Oe,dc}} + \Delta H_{\text{FLT,dc}}) \sin\varphi, \tag{2}$$

where φ is the angle between the external magnetic field and the current. As the device is much wider than its thickness, the Oersted field by the charge current is $-[(\Delta j_{c,\text{NM}} d_{\text{NM}})/2]$ if a direct current uniformly flows in the NM layer, where $j_{c,\text{NM}}$ and d_{NM} are the electrical current density and the thickness of the NM layer. The effective field of FLT is $-\xi_{\text{FL}}[\hbar/(2e)][1/(\mu_0 M_s t_{\text{FM}}^{\text{eff}})]\Delta j_{c,\text{NM}}$, where $\hbar$, e, $\mu_0 M_s$, and $t_{\text{FM}}^{\text{eff}}$ are Plank's constant, the electronic charge, the saturation magnetization, and the effective thickness of the FM layer, respectively [18]. With a FM/NM bilayer structure, $\Delta j_{c,\text{NM}}$ is $\Delta I[(R_{\text{FM}})/(R_{\text{FM}} + R_{\text{NM}})][1/(A_{C,\text{NM}})]$, where R_{FM}, R_{NM}, and $A_{C,\text{NM}}$ are the resistance of the FM layer and the resistance and the cross section of the NM layer, respectively. Using the above equations, Eq. (2) is expressed as

$$\xi_{\text{FL}} = \left(\frac{2e}{\hbar}\right)\left(\frac{\Delta H_R}{\Delta I}\frac{1}{\sin\varphi}\frac{R_{\text{FM}} + R_{\text{NM}}}{R_{\text{FM}}}A_{C,\text{NM}}S - \frac{d_{\text{NM}}}{2}\right) \times \mu_0 M_s t_{\text{FM}}^{\text{eff}}. \tag{3}$$

If we obtain the slope of the resonance field for a dc applied to the device, FLTE can be estimated with the additional information about the dimensions and the dc resistivity of each layer. Here, S is 1 or -1 when the device has the structure FM/NM, as in Fig. 1(a), or NM/FM.

We simulate a macrospin system in a dc-tuned ST FMR with the Landau-Lifshitz equation containing the Slonczewski torques [19–21]. We investigate the magnetization dynamics with the spin-torque efficiency

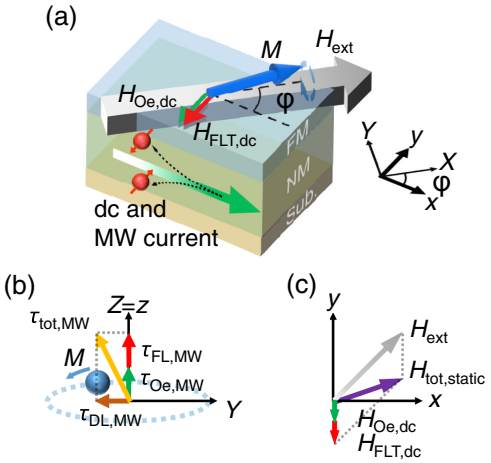

FIG. 1. Schematic diagrams of a dc-tuned ST FMR. (a) SHE and dc-tuned ST FMR. The x-y and X-Y planes are in the same plane, the plane of the film. In the NM layer, the dc and MW currents along the x axis generate the spin current along the z axis. The magnetization (M) precessional motion around the external magnetic field (H_{ext}) is applied to a dc flow at a certain angle (φ). The Oersted field ($\text{H}_{\text{Oe,dc}}$) and the effective field of FLT ($H_{\text{FLT,dc}}$) by a dc are indicated. (b) Torques generated from a MW current in ST FMR. The projected vectors of FLT ($\tau_{\text{FL,MW}}$), DLT ($\tau_{\text{DL,MW}}$), and the Oersted torque ($\tau_{\text{Oe,MW}}$) by a MW current are drawn in the Y-Z plane. The precessional motion of magnetization (M) is also projected on the same plane. The X axis is the direction of the external magnetic field. The precessional phase of magnetization is determined according to the direction of the total torque ($\tau_{\text{tot,MW}}$) on the Y-Z plane. (c) Static fields in dc-tuned ST FMR. Vectors of H_{ext}, $\text{H}_{\text{Oe,dc}}$ and the $H_{\text{FLT,dc}}$ by a dc are drawn on the x-y plane. The sum of these fields is the total static field ($H_{\text{tot static}}$) applied to the magnetization. All pictures are drawn under the assumption that FLTE and DLTE are positive.

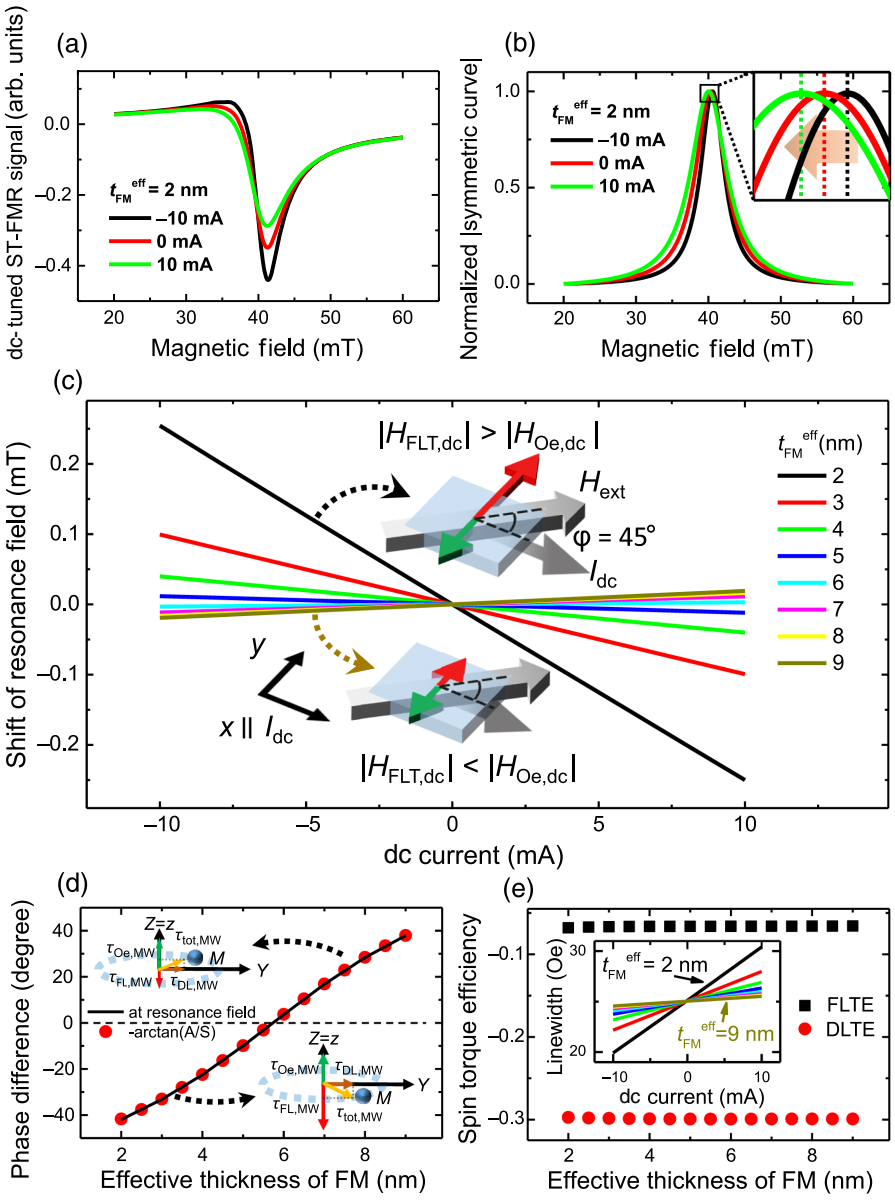

FIG. 2. Simulation results for a dc-tuned ST FMR. (a) Simulated spectra for dc-tuned ST FMR at −10, 0, and 10 mA dc with $t_{FM}^{eff} = 2$ nm. (b) Normalizations of the absolute symmetric curves of (a). (Inset) Enlargement near the peaks. (c) Shifted resonance field over the applied dc at each FM layer. Schematic diagrams of H_{ext}, $H_{FLT,dc}$, $H_{Oe,dc}$, and I_{dc} are also shown when $H_{FLT,dc}$ is larger or smaller than $H_{Oe,dc}$. (d) The phase difference between the magnetization and the Oersted field along the y axis at the resonance field. Phase differences are also shown through the ratio of antisymmetric and symmetric Lorentzians at each FM layer. The schematic diagrams of FLT ($\tau_{FL,MW}$), DLT ($\tau_{DL,MW}$), and the Oersted torque ($\tau_{Oe,MW}$) by MW current are also shown when $\tau_{FL,MW}$ is larger or smaller than $\tau_{Oe,MW}$. (e) Calculated FLTE and DLTE by MOR and MOD at each FM layer. (Inset) Linewidth as a function of the dc for different FM thicknesses.

($\xi_{DL} = -0.3$ and $\xi_{FL} = -0.066$) of the NM layer with respect to the thin-film thickness, the external magnetic field, the MW current, and the dc. We calculate the ST-FMR signal (on an arbitrary scale) by multiplying the magnetization along the y axis by the MW current [3].

Figure 2(a) shows the spectra of the dc-tuned ST FMR at –10, 0, and 10 mA dc with $t_{FM}^{eff} = 2$ nm. There are obvious changes in intensity and linewidth in the spectra because DLT by dc acts like a damping torque [17]. After these spectra are fitted with symmetric and antisymmetric Lorentzians, only normalizations of the absolute symmetric curves are depicted in Fig. 2(b) [5]. The inset in Fig. 2(b) presents an enlarged view of the peaks of these spectra; the resonance field apparently decreases when the applied dc increases.

Only the effective field of FLT by a dc can lead to a decrease in the resonance field because the effective field by negative FLTE has a component parallel to the external magnetic field. By contrast, the Oersted field has a component that is antiparallel to the external magnetic field. This field configuration results in an increase in the resonance field with an increase in dc, which is the opposite of the effective field by negative FLTE. In Fig. 2(b), because the effective field of FLT is larger than the Oersted field, the resonance field finally decreases.

The shifted resonance fields are depicted in Fig. 2(c) as a function of the dc for each layer. For thin FM layers ($t_{FM}^{eff} < 6$ nm), the resonance field decreases with an increasing current. However, in $t_{FM}^{eff} > 6$ nm, the slopes of the shifted resonance field are positive because the effective field of FLT is smaller than the Oersted field.

This competition between the Oersted field and the effective field of the FLT can be observed with application of the MW current over various FM thicknesses. The

oscillating total torque consisting of FLT, DLT, and the Oersted torque by the MW current resonates the magnetization in the ST-FMR experiment [Fig. 1(b)]. With the increase in the FM layer, the torque in the out-of-plane direction (the sum of the FLT and the Oersted torque) changes from negative to positive at the resonant field when the MW current along the x axis is positive. This is the case because the relative intensity between the two torques changes as depicted in Fig. 2(d), which leads to the change in the magnetization precession phase. The phase difference $[\Delta\psi(t_{\mathrm{FM}}^{\mathrm{eff}})]$ at the resonance field and a certain FM layer is defined by subtracting the oscillating phase of the Oersted torque along the z axis $[\psi_{\mathrm{Oe},z}(t_{\mathrm{FM}}^{\mathrm{eff}})]$ from the precession phase of magnetization along the Y axis $[\psi_{m,Y}(t_{\mathrm{FM}}^{\mathrm{eff}})]$ and is expressed as

$$\Delta\psi(t_{\mathrm{FM}}^{\mathrm{eff}}) = \psi_{m,Y}(t_{\mathrm{FM}}^{\mathrm{eff}}) - \psi_{\mathrm{Oe},z}(t_{\mathrm{FM}}^{\mathrm{eff}}). \quad (4)$$

The phase differences for various FM thicknesses are shown in Fig. 2(d). With increasing the FM layer, the phase difference increases and reaches 0° between $t_{\mathrm{FM}}^{\mathrm{eff}} = 5.5$ and 6 nm. At this FM thickness, only DLT resonates the magnetization because FLT and the Oersted torque cancel each other out.

In the ST-FMR experiment, the dc voltage originates from mixing the oscillating resistance of the device with MW current [3]. Along the y axis, the oscillating longitudinal resistance is mainly caused by the precession of magnetization. The MW current generates the oscillating Oersted field with a 0° or 180° phase difference, depending on the sample structure. Thus, the phase difference between the longitudinal resistance and the MW current is related to the phase difference between the precessional phase of magnetization and the torque by the Oersted field. Because the detection mechanism of ST FMR is the same as a single-axis detection of a homodyne quadrature scheme, the ratio between the antisymmetric and symmetric Lorentzians in the line-shape analysis is related to the phase difference between the mixing components [22,23]. Therefore, in ST FMR, the phase difference $[\Delta\psi(t_{\mathrm{FM}}^{\mathrm{eff}})]$ can be expressed as the ratio between the antisymmetric (A) and symmetric (S) Lorentzians as

$$\Delta\psi(t_{\mathrm{FM}}^{\mathrm{eff}}) = -\tan^{-1}\left(\frac{A}{S}\right). \quad (5)$$

Therefore, the ST-FMR measurements of spin-torque efficiencies analyze the modulation-of-precession phase (MOP) in magnetization dynamics in various FM thicknesses. The phase difference calculated by Eq. (5) is also depicted in Fig. 2(d).

Using Eq. (3) and the slopes in Fig. 2(c), FLTE is calculated for each FM layer [see Fig. 2(e)]. For all FM layers, the estimated values of FLTE are nearly –0.066, which is the same as the input parameter of the simulation. In addition, DLTE is calculated from the change in linewidth in the inset of Fig. 2(e), and shows the same behavior with the input parameter [17].

To observe SOT effects generated from the direct and MW currents in ST FMR, we perform a dc-tuned ST FMR in the trilayer system $W(5\ \mathrm{nm})/Co_4Fe_4B_2(t_{\mathrm{FM}})/Ta(1\ \mathrm{nm})(t_{\mathrm{FM}} = 2.5\text{–}9\ \mathrm{nm})$ [19]. The amplitude of the MW signal is modulated with several hundred hertz for lock-in detection. By a bias tee, direct and MW currents are applied to a device to resonate magnetization and enhance the SOT. In the dc-tuned ST FMR, the MW power is 10–20 dBm with 4.5–7 GHz.

Figure 3(a) shows the resonance field with $t_{\mathrm{FM}}^{\mathrm{eff}} = 2.06$ nm in dc-tuned ST FMR. An offset of about 0.2 mT is found at $I = 0$ mA, which originates from inaccurate calibration of the external magnetic field. We depict the even and odd components of Fig. 3(a) in Figs. 3(b) and 3(c) using $\{[H_R(I) - H_R(0)] \pm [H_R(-I) - H_R(0)]\}/2$, where a (+) or (–) sign describes an even or odd component.

In Fig. 3(b), the even components fit well with the quadratic term. Because the increase of temperature by Joule heating depends on the intensity of the direct current and not on the direction of the direct current, this thermal effect should be reflected in the even component of the shifted resonance field. From the shifted resonance field of about 0.3 mT at $I = \pm 7$ mA, it can be estimated that the effective magnetization changes by about 1% using the Kittel formula [24]. From Bloch's law $(M_S(T) = M_S(0)[1 - (T/T_C)^{1.7}])$, the increase in temperature can be estimated to be about 10 K on the assumption that the Curie temperature (T_C) of the $Co_4Fe_4B_2$ layer is 900 K [25]. With this small change, the effective magnetization is linearly proportional to the resonance field and temperature. A dc is applied to the device and raises the temperature (T) of the FM layer because of power dissipation (P_{diss}) by Joule heating. Therefore, the shifted resonance field should increase with the square of the applied dc $[\Delta H_R \propto 4\pi\Delta M_{\mathrm{eff}} \propto \Delta T \propto \Delta P_{\mathrm{diss}} \propto \Delta(I)^2]$. We conduct additional ST-FMR experiments at varying temperatures in order to confirm that the quadratic shift of the resonance field comes from the thermal effect of the direct current. In the experiment, the resonance field is linearly shifted with an increase of temperature. The resultant shift of the resonance field is 0.3 mT for a temperature rise of 12(±1) K [19].

Odd components in Fig. 3(c) fit well with the linear curve and are symmetric along the y axis. The shifted resonance fields with various FM thicknesses are shown in Fig. 3(d). With an increase in the FM layer, the slope decreases and changes its sign near $t_{\mathrm{FM}}^{\mathrm{eff}} = 4.56$ nm. Simultaneously, at the phase difference point shown in Fig. 3(e), the magnetization phase also changes from negative to positive. At this thickness, the vector sums of torques and fields of the Oersted and FLT effects generated by the dc and MW currents change their direction.

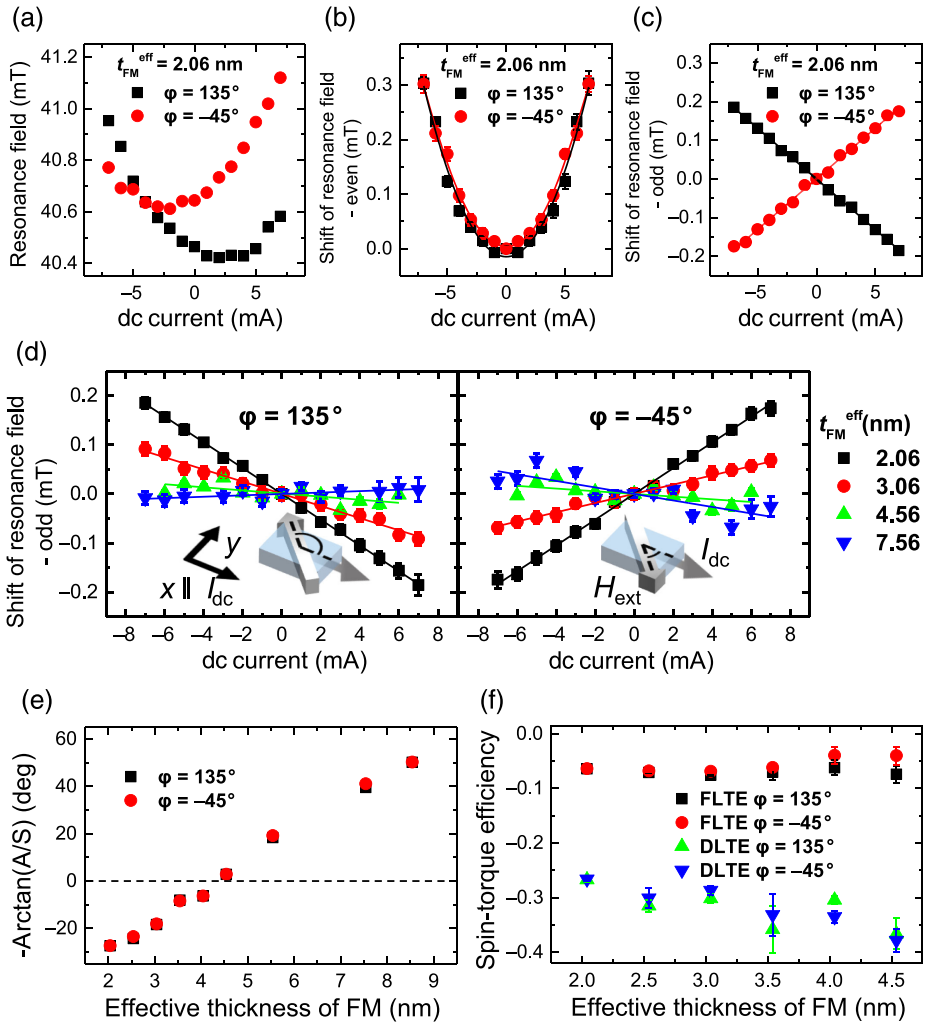

FIG. 3. Experimental results for the dc-tuned ST FMR (a) Resonance field as a function of the dc in each ST-FMR spectrum with $t_{FM}^{eff} = 2.06$ nm. (b),(c) Even and odd components of the shifted resonance field of (a). The lines are the fitting results for quadratic and linear curves. (d) Shifted resonance field as a function of dc magnitude at each FM layer. The lines are the linear fitting results for each angle and FM thickness. (e) The phase difference obtained from the ratio between the antisymmetric and symmetric Lorentzians with various FM thicknesses at $I = 0$ mA. In all FM thickness, the error bars are smaller than the data points. (f) FLTE and DLTE estimated from MOR and MOD in dc-tuned ST FMR for each angle and FM thickness.

FLTE and DLTE are calculated by MOR and modulation of damping (MOD) in the dc-tuned ST FMR [see Fig. 3(f)]. We obtain resistivities of each layer from several sheet resistances of $W/Co_4Fe_4B_2$ regarded as two parallel resistors. The inverse of the total sheet resistance versus the FM thickness shows a nearly linear curve. These fitting results would lead to some errors in calculating the DLTE and FLTE of each FM thickness. But this error is smaller than 5% [19,26–30]. As FM thickness increases, the error in estimating FLTE gradually increases and reaches about 30% of the data value at $t_{FM}^{eff} = 4.56$ nm because the signal-to-noise ratio decreases in each spectrum due to reduced MW current density. Above $t_{FM}^{eff} = 5$ nm, we do not draw SOT efficiencies because the error is larger than 50% of the data value and the deviation between the two directions of the magnetic field is apparent. Thus, we believe that the obtained data value does not indicate the real SOT efficiency above $t_{FM}^{eff} = 5$ nm. The average value of FLTE is $-0.068(\pm 0.005)$. In DLTE, errors with $t_{FM}^{eff} < 5$ nm are below 10% of its value, except for $t_{FM}^{eff} = 3.56$ nm, but DLTE continuously increases with an increasing FM thickness. The average value of DLTE is $-0.318(\pm 0.037)$. In MOP ST FMR, FLTE and DLTE are $-0.052(\pm 0.002)$ and $-0.310(\pm 0.023)$.

III. CONCLUSION

In this paper, we obtain fieldlike ST efficiency by manipulating a resonance field in both simulation and experiment for a dc-tuned ST FMR. With negative fieldlike-torque efficiency, the effective field of fieldlike-torque efficiency is antiparallel to the Oersted field by current. Because these fields are added to the external static magnetic field, the resonance field is shifted with a dc. Moreover, as the thickness of the ferromagnetic layer increases, a relative ratio between the effective field of the fieldlike torque and the Oersted field varies, resulting in a change in the slope of the shifted resonance field and precession phase of the magnetization. The shifted phase is reflected in the ratio between the antisymmetric and symmetric Lorentzians. Additionally, we observe a quadratic change in the resonance field because of Joule heating by the dc.

ACKNOWLEDGMENTS

This research was supported by Future Materials Discovery Program through the National Research Foundation of Korea (NRF), funded by the Ministry of Science and ICT (MSI) (Grant No. 2015M3D1A1070462), and by the National Research Council of Science and Technology (NST) (Grant No. CAP-16-01-KIST) through MSIP.

[1] M. Harder, Y. Gui, and C.-M. Hu, Electrical detection of magnetization dynamics via spin rectification effects, Phys. Rep. **661**, 1 (2016).

[2] A. A. Tulapurkar, Y. Suzuki, A. Fukushima, H. Kubota, H. Maehara, K. Tsunekawa, D. D. Djayaprawira, N. Watanabe, and S. Yuasa, Spin-torque diode effect in magnetic tunnel junctions, Nature (London) **438**, 339 (2005).

[3] J. C. Sankey, Y.-T. Cui, J. Z. Sun, J. C. Slonczewski, R. A. Buhrman, and D. C. Ralph, Measurement of the spin-transfer-torque vector in magnetic tunnel junctions, Nat. Phys. **4**, 67 (2008).

[4] H. Kubota, A. Fukushima, K. Yakushiji, T. Nagahama, S. Yuasa, K. Ando, H. Maehara, Y. Nagamine, K. Tsunekawa, D. D. Djayaprawira, N. Watanabe, and Y. Suzuki, Quantitative measurement of voltage dependence of spin-transfer torque in MgO-based magnetic tunnel junctions, Nat. Phys. **4**, 37 (2008).

[5] L. Liu, T. Moriyama, D. C. Ralph, and R. A. Buhrman, Spin-Torque Ferromagnetic Resonance Induced by the Spin Hall Effect, Phys. Rev. Lett. **106**, 036601 (2011).

[6] M. Harder, Z. X. Cao, Y. S. Gui, X. L. Fan, and C.-M. Hu, Analysis of the line shape of electrically detected ferromagnetic resonance, Phys. Rev. B **84**, 054423 (2011).

[7] J. E. Hirsch, Spin Hall Effect, Phys. Rev. Lett. **83**, 1834 (1999).

[8] P. Gambardella and I. M. Miron, Current-induced spin-orbit torques, Phil. Trans. R. Soc. A **369**, 3175 (2011).

[9] J. Sinova, S. O. Valenzuela, J. Wunderlich, C. H. Back, and T. Jungwirth, Spin Hall effects, Rev. Mod. Phys. **87**, 1213 (2015).

[10] K. Garello, I. M. Miron, C. O. Avci, F. Freimuth, Y. Mokrousov, S. Blgel, S. Auffret, O. Boulle, G. Gaudin, and P. Gambardella, Symmetry and magnitude of spin-orbit torques in ferromagnetic heterostructures, Nat. Nanotechnol. **8**, 587 (2013).

[11] X. Fan, J. Wu, Y. Chen, M. J. Jerry, H. Zhang, and J. Q. Xiao, Observation of the nonlocal spin-orbital effective field, Nat. Commun. **4**, 1799 (2013).

[12] C.-F. Pai, Y. Ou, L. H. Vilela-Leo, D. C. Ralph, and R. A. Buhrman, Dependence of the efficiency of spin Hall torque on the transparency of Pt/ferromagnetic layer interfaces, Phys. Rev. B **92**, 064426 (2015).

[13] Y. Wang, P. Deorani, K. Banerjee, N. Koirala, M. Brahlek, S. Oh, and H. Yang, Topological Surface States Originated Spin-Orbit Torques in Bi_2Se_3, Phys. Rev. Lett. **114**, 257202 (2015).

[14] K.-U. Demasius, T. Phung, W. Zhang, B. P. Hughes, S.-H. Yang, A. Kellock, W. Han, A. Pushp, and S. S. P. Parkin, Enhanced spin-orbit torques by oxygen incorporation in tungsten films, Nat. Commun. **7**, 10644 (2016).

[15] K. Kondou, H. Sukegawa, S. Kasai, S. Mitani, Y. Niimi, and Y. Otani, Influence of inverse spin Hall effect in spin-torque ferromagnetic resonance measurements, Appl. Phys. Express **9**, 023002 (2016).

[16] A. Kumar, S. Akansel, H. Stopfel, M. Fazlali, J. Kerman, R. Brucas, and P. Svedlindh, Spin transfer torque ferromagnetic resonance induced spin pumping in the Fe/Pd bilayer system, Phys. Rev. B **95**, 064406 (2017).

[17] K. Ando, S. Takahashi, K. Harii, K. Sasage, J. Ieda, S. Maekawa, and E. Saitoh, Electric Manipulation of Spin Relaxation Using the Spin Hall Effect, Phys. Rev. Lett. **101**, 036601 (2008).

[18] A. V. Khvalkovskiy, V. Cros, D. Apalkov, V. Nikitin, M. Krounbi, K. A. Zvezdin, A. Anane, J. Grollier, and A. Fert, Matching domain-wall configuration and spin-orbit torques for efficient domain-wall motion, Phys. Rev. B **87**, 020402 (2013).

[19] See Supplemental Material at http://link.aps.org/supplemental/10.1103/PhysRevApplied.9.054035 for the simulation, sample growth, and characterization and analysis of the thermal effect in ST FMR.

[20] J. C. Slonczewski, Current-driven excitation of magnetic multilayers, J. Magn. Magn. Mater. **159**, L1 (1996).

[21] A. Vansteenkiste, J. Leliaert, M. Dvornik, M. Helsen, F. Garcia-Sanchez, and B. Van, Waeyenberge, The design and verification of MUMAX3, AIP Adv. **4**, 107133 (2014).

[22] A. G. Marshall and D. C. Roe, Dispersion versus absorption: Spectral line shape analysis for radiofrequency and microwave spectrometry, Anal. Chem. **50**, 756 (1978).

[23] F. Montigny, K. Elbayed, J. Brondeau, and D. Canet, Automatic phase correction of Fourier transform nuclear magnetic resonance spectroscopy data and estimation of peak area by fitting to a Lorentzian shape, Anal. Chem. **62**, 864 (1990).

[24] C. Kittel, On the theory of ferromagnetic resonance absorption, Phys. Rev. **73**, 155 (1948).

[25] K.-M. Lee, J. W. Choi, J. Sok, and B.-C. Min, Temperature dependence of the interfacial magnetic anisotropy in W/CoFeB/MgO, AIP Adv. **7**, 065107 (2017).

[26] Q. Hao and G. Xiao, Giant Spin Hall Effect and Switching Induced by Spin-Transfer Torque in a $W/Co_{40}Fe_{40}B_{20}/MgO$ Structure with Perpendicular Magnetic Anisotropy, Phys. Rev. Applied **3**, 034009 (2015).

[27] J.-S. Lee, J. Cho, and C.-Y. You, Growth and characterization of α and β-phase tungsten films on various substrates, J. Vac. Sci. Technol. A **34**, 021502 (2016).

[28] Q. Hao, W. Chen, and G. Xiao, Beta (β) tungsten thin films: Structure, electron transport, and giant spin Hall effect, Appl. Phys. Lett. **106**, 182403 (2015).

[29] L. Liu, C.-F. Pai, Y. Li, H. W. Tseng, D. C. Ralph, and R. A. Buhrman, Spin-torque switching with the giant spin Hall effect of tantalum, Science **336**, 555 (2012).

[30] S. U. Jen, Y. D. Yao, Y. T. Chen, J. M. Wu, C. C. Lee, T. L. Tsai, and Y. C. Chang, Magnetic and electrical properties of amorphous CoFeB films, J. Appl. Phys. **99**, 053701 (2006).